技術論文

Abnormal Grain Growth and Recrystallization in Al-Mg Alloy AA5182 Following Hot Deformation

Jung-Kuei Chang　Ken Takata　Koji Ichitani　Eric M. Taleff

Abstract : Abnormally large grains have been observed in Al-Mg alloy AA5182 sheet material after forming at elevated temperature, and the reduced yield strength that results in a practical problem for commercial hot-forming operations. The process by which abnormal grains are produced is investigated through controlled hot tensile testing to reproduce the microstructures of interest. Abnormal grains are shown to develop strictly during static annealing or cooling following hot deformation; the formation of abnormal grains is suppressed during plastic straining. Abnormal grains grow by static abnormal grain growth (SAGG), which becomes a discontinuous recrystallization process when abnormal grains meet to form a fully recrystallized microstructure. Nuclei which grow under SAGG are produced during hot deformation by the geometric dynamic recrystallization (GDRX) process. The mechanism through which a normally continuous recrystallization process, GDRX, may be interrupted by a discontinuous process, SAGG, is discussed.

1. INTRODUCTION

Commercial aluminum alloys which contain magnesium as the primary alloying addition, the 5000-series alloys, have gained importance through the hot forming of structural components, particularly for the transportation industry in its drive toward reduced vehicle mass. Among the most common materials used in commercial superplastic forming (SPF) operations is fine-grained AA5083 sheet [1)~4)]. Fine-grained AA5083 exhibits a low flow stress and very high tensile ductility, classical superplastic behavior [5), 6)], when deformed under the grain-boundary-sliding (GBS) creep mechanism. GBS creep occurs at slow strain rates and high temperatures, which are the conditions used in SPF operations. As strain rate increases and temperature decreases, deformation in fine-grained AA5083 transitions to control by solute-drag (SD) creep [7)]. Although the high strain-rate sensitivity of SD creep ($m \approx 0.25$ to 0.33) provides less tensile ductility than is possible under GBS creep ($m \approx 0.5$), ductility is still sufficiently enhanced to form quite complex components. The quick-plastic forming (QPF) process takes advantage of SD creep to form fine-grained AA5083 sheet at faster rates and lower temperatures than possible in traditional SPF operations [8)]. It has been shown that SD creep can provide enhanced ductility in even coarse-grained Al-Mg alloys, which are not subject to deformation by GBS creep at the temperatures and strain rates of interest for commercial forming operations [9)~16)]. Non-superplastic varieties of commercial Al-Mg alloys are now used in commercial production of structural components by hot forming processes such as high-cycle blow forming [17), 18)] and hot bulge forming [19), 20)]. The use of non-superplastic commercial Al-Mg materials considerably expands the opportunities to use hot forming for production of aluminum structural components. However, a critical problem was encountered in hot-forming trials with these materials, the development of abnormal grains [18)~20)]. Abnormal grains are isolated large grains in an otherwise much finer microstructure [21), 22)]. Abnormal grains can significantly lower yield strength through the Hall-Petch effect, which can render a formed part unusable.

Fukuchi *et al*. encountered abnormal grains in alloy AA5052 with a moderate initial grain size during trials of hot bulge forming [19)]. This problem was addressed by modifying the alloy with a small Cr addition [20)], which assists the pinning of grain boundaries. A similar issue of abnormal grain production was encountered during hot blow forming of AA5182 sheet

with a moderate grain size, and this was addressed by Kazama *et al*. through a similarly slight alloy modification [18]. Recrystallization to very coarse grain sizes in fine-grained AA5083 material subjected to tensile testing at elevated temperatures and strain rates characteristic of the QPF process was recently investigated by Agarwal *et al*. [23] Dynamic recrystallization by particle-stimulated nucleation (PSN) of recrystallization was identified as the most likely cause of coarse grains observed in the AA5083 material after hot tensile straining. However, this mechanism is less likely in the AA5052 and AA5182 materials because of their lower Mn + Cr alloy contents, which provide fewer pro-eutectic products, the hard intermetallic particles responsible for PSN of recrystallization in AA5083 material. The cause of abnormal grains developed by hot deformation of AA5052 and AA5182 materials with moderate grain sizes remains elusive.

The goals of the present investigation are to: (1) reproduce abnormal grains in AA5182 material through elevated-temperature tensile testing at a controlled strain rate and (2) identify the mechanism responsible for formation of these abnormal grains. Because this investigation deals with the complex phenomena of recrystallization and grain growth, a brief discussion of terminology is in order. Wherever possible, the most modern accepted terminology for recrystallization phenomena is used. This includes categorization of recrystallization as static or dynamic and as continuous or discontinuous [21), 24), 25)]. Distinction between recrystallization and grain growth is not always possible [21)], making it quite important to clearly define how these terms are used. The term grain growth is herein applied to any case for which a grain increases in size, regardless of whether it grows into a deformed or an undeformed microstructure. The practical ramification of this definition occurs when a new grain, formed from a nucleus of recrystallization, grows into a deformed microstructure. In this case, grain growth is considered a part of the discontinuous recrystallization process, which allows a clear description of the phenomena observed in this investigation.

2 EXPERIMENTAL PROCEDURES

An AA5182 aluminum alloy sheet material was produced for this investigation by direct-chill casting followed by homogenization, hot-rolling to a thickness of 6 mm, cold-rolling to a final thickness of 3 mm and then annealing at 530°C for 10 min. The composition of the AA5182 material is provided in **Table 1** Four types of experiments were conducted using this material: (1) annealing of the as-received material, (2) tensile tests to fracture at elevated temperature, (3) tensile tests to a predetermined elongation at elevated temperature, immediately followed by controlled cooling, and (4) static annealing of specimens following tensile testing and controlled cooling. Microstructures of the as-received and tested materials were examined using optical microscopy (OM), scanning-electron microscopy (SEM) and electron back-scatter diffraction (EBSD).

Table 1 Chemical composition of the AA5182 material is given in weight percent.

Si	Fe	Cu	Mn	Mg	Cr	Zn	Ti	Al
0.11	0.18	0.10	0.36	4.40	0.04	0.02	0.02	bal

Annealing experiments were conducted in a pre-heated box furnace with resistance heating elements. Specimen temperature was monitored during annealing with a shielded type-K thermocouple adjacent to the specimen. Static annealing tests of the as-received material were conducted for the conditions shown in **Table 2**, and grain sizes after annealing were measured using optical microscopy. All grain sizes reported in this study are lineal-intercept sizes measured in accordance with the ASTM E 112 standard [26)]. Metallographic specimens for optical microscopy were prepared by standard grinding and polishing techniques prior to etching with Barker's reagent (5 ml HBF in 100 ml H_2O) through an electrolytic etching procedure at 25 V for approximately 60 s. Etched specimens were observed using polarizing filters to produce color contrast between grains.

Table 2 Lineal intercept grain size, d, following static annealing of the as-received AA5182 sheet at temperature T for time t_a is given. The standard deviation on grain size measurements is approximately 2 μm.

T, °C	As received	500	500	500	500	500	525	525	550
t_a, hr.	0	1	3	6	12	24	1	12	1
d, μm	17	16	18	18	16	17	18	>1000	>1000

Tensile specimens were machined from the AA5182 sheet into a dog-bone geometry with a gage width of 6 mm, a gage length of 25 mm and a 6-mm shoulder radius between the grip and gage regions. The tensile axis was parallel to the rolling direction for all specimens, and thickness was that of the as-received sheet (3 mm). Specimens were tested in rigid grips, which load the specimen shoulders outside the gage region. Tensile tests to fracture were conducted at temperatures of 300, 350 and 400°C with constant true-

strain rates of 10^{-3}, 3×10^{-3}, 10^{-2} and 3×10^{-2} s^{-1}. Tensile tests to a pre-determined elongation of 180% were conducted at a temperature of 400°C and a constant true-strain rate of 3×10^{-2} s^{-1}. Specimen temperature was controlled using a three-zone resistance furnace and was monitored at each end of the gage length using separate type-K thermocouples. Temperature was held to within approximately ± 1.5°C of the specified testing temperature along the entire specimen length. Specimens were tested in tension at constant true-strain rates using a computer-controlled, servo-hydraulic test system. To achieve a constant true-strain rate, displacement rate was specified as a function of time assuming conservation of volume and uniform deformation in the specimen gage region. Specimens tested to fracture were allowed to air cool in the opened furnace following tensile testing. Specimens tested to a predetermined elongation of 180% were cooled after tensile testing either by air cooling in the opened furnace (AC) or by water quenching of the gage section in a water spray (WQ) immediately upon completion of tensile straining. Selected specimens were annealed at 400°C for one hour in a box furnace following tensile testing to 180% elongation. Specimen conditions produced are summarized in **Table 3**.

Table 3 Experimental conditions for microstructural studies of the AA5182 sheet material are given. Tensile elongation, e, is in percent.

Condition	Tensile test conditions				Subsequent anneal	
	T, °C	$\dot{\varepsilon}$, s	*e*, %	Cooling	*T*, °C	*t*, hrs.
AC	400	3×10^{-2}	180	AC		
AC + A	400	3×10^{-2}	180	AC	400	1.0
WQ	400	3×10^{-2}	180	WQ		
WQ + A	400	3×10^{-2}	180	WQ	400	1.0

AC :air cooled in open furnace immediately after testing
WQ :water quenched immediately after testing
+ A :subsequently annealed

Each specimen tested to an elongation of 180% exhibited a diffuse neck. Width and thickness were measured at 5-mm increments along the gage lengths of these specimens. These data were used to calculate the following: (1) cross-sectional area, A; (2) reduction-in-area, $q = (A_0 - A)/A_0$, where A_0 is original cross-sectional area; (3) R value, the ratio of width to thickness strains, which generally varied within the range of 0.8 to 0.9; (4) and the true strain from area reduction, $\varepsilon = \ln(A_0/A)$, at each 5-mm increment along the gage length. Tested specimens were sectioned for observation of microstructure in the plane containing the rolling direction (RD), identical with the longitudinal (L) direction, and the long-transverse (LT) direction. The rolling direction is the same as the tensile direction in coupons tested for this study. All photomicrographs are presented with the RD horizontal and the LT direction vertical. Specimens observed by OM were polished and electrolytically etched, as described previously, and were observed using polarizing filters. This technique reveals both grains and the subgrains which evolve during creep deformation. High-resolution, composite images of large specimen areas were created by digitally stitching together numerous individual photomicrographs. These high-resolution, composite images facilitated the examination of microstructure across regions of diffuse necking, which contain mild strain gradients. Specimens observed using the EBSD technique were prepared by ion milling with Ar. One specimen observed in the WQ condition by EBSD, see Table 3, was subsequently annealed at 400°C for one hour in a vacuum induction furnace, which provided rapid cooling after annealing, and was again examined using EBSD across the same area. The measured values of R and q were used to calculate local true strain from width measurements of tested specimens subjected to metallographic observation. In this manner, true strain at the position of each microstructure measurement was determined.

3 RESULTS

3.1 Grain Stability

The microstructure of as-received AA5182 sheet material is shown in **Fig.1** (a). This material has a recrystallized, equiaxed grain structure with an average lineal-intercept grain size of 17 μm. An example of an abnormal grain produced by tensile testing is shown in Fig.1(b). This example effectively duplicates the abnormal grains previously reported in AA5182 sheet material after hot forming [18]. In order to investigate the stability of microstructure in this material, static annealing experiments were conducted at the temperatures and times indicated in Table 2. Grain size was measured following each annealing treatment, and these measurements are reported in Table 2. The standard deviation on all grain size measurements is approximately 2 μm. Grain size is stable at 500°C for times up to at least 24 hrs. At 525°C, grain size is generally stable for up to approximately one hour. Abnormal grains grew in specimens annealed at 525°C for more than one hour. Annealing for 12 hrs. at 525°C resulted in coarse grains of greater than 1 mm in size throughout the specimen, as did annealing at 550°C for only one hour. These data indicate that the grain size of this material is stable during static annealing at the test temperatures used for mechanical testing, 300 up to 400°C.

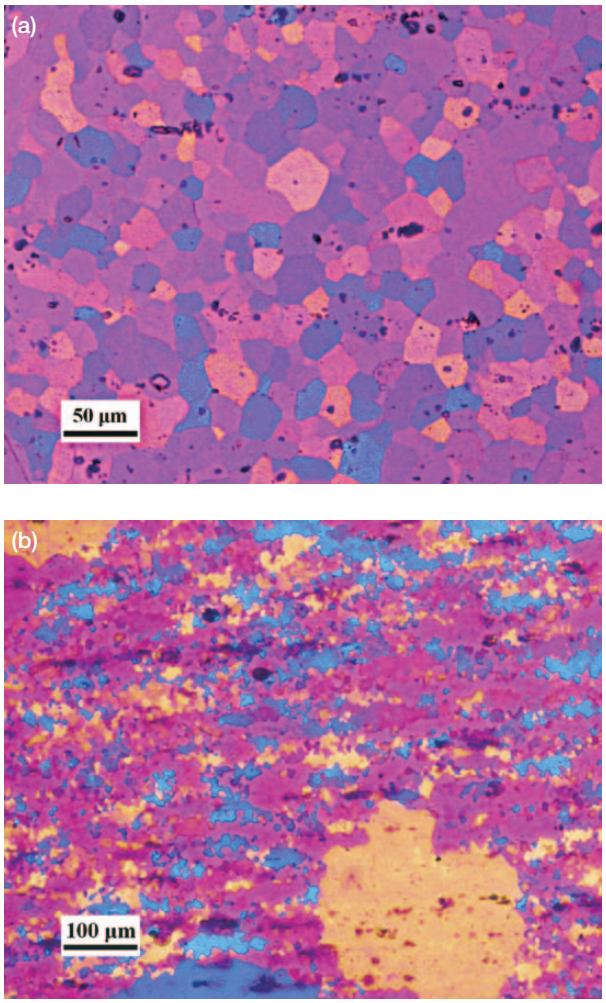

Fig.1 Optical photomicrographs are shown of (a) the as-received AA5182 sheet material and (b) an abnormal grain formed during air cooling following a tensile test at 400°C and 3 × 10^{-2} s^{-1}. The local true strain from area reduction at the location of (b) is approximately 1.25.
(a) as-received
(b) after testing

3.2 Deformation Response

The results of tensile elongation-to-fracture experiments are presented in **Fig.2** and **Fig.3**. Fig.2(a) presents true-strain rate as a function of true stress, at a true strain of ε = 0.2, on dual-logarithmic scales. The slope of these data is equal to the stress exponent, n, of the phenomenological equation for creep [27],

$$\dot{\varepsilon} = A \exp\left(-\frac{Q_c}{RT}\right)\left(\frac{\sigma}{E}\right)^n \qquad (1)$$

where A is a material-dependent constant, Q_c is the activation energy for creep, R is the universal gas constant, T is absolute temperature and E is the dynamic, unrelaxed elastic modulus. The stress exponent is the inverse of strain-rate sensitivity, $n = 1/m$. The value of $n \approx 4$ is known from a number of prior studies to be indicative of SD creep in commercial Al-Mg alloys, which contain Mn [7), 9), 11), 13), 16), 28)~31)]. This stress exponent is slightly higher than the value of $n = 3$ observed in low-impurity alloys [32), 33)] because of an increased dependence of dislocation glide velocity on stress in the commercial materials [29)]. Solute-drag creep is a deformation mechanism which occurs when an "atmosphere" of solute atoms interacts with dislocations to significantly slow the rate of dislocation glide, and Al-Mg alloys offer a classical example of this creep mechanism [34)~37)]. This makes SD creep largely insensitive to grain size [11)]. The activation energy for creep was measured to be approximately Q_c = 136 kJ/mol, which is the expected value for solute-drag creep in Al-Mg alloys and is approximately equal to the activation energy for diffusion of Mg in Al.

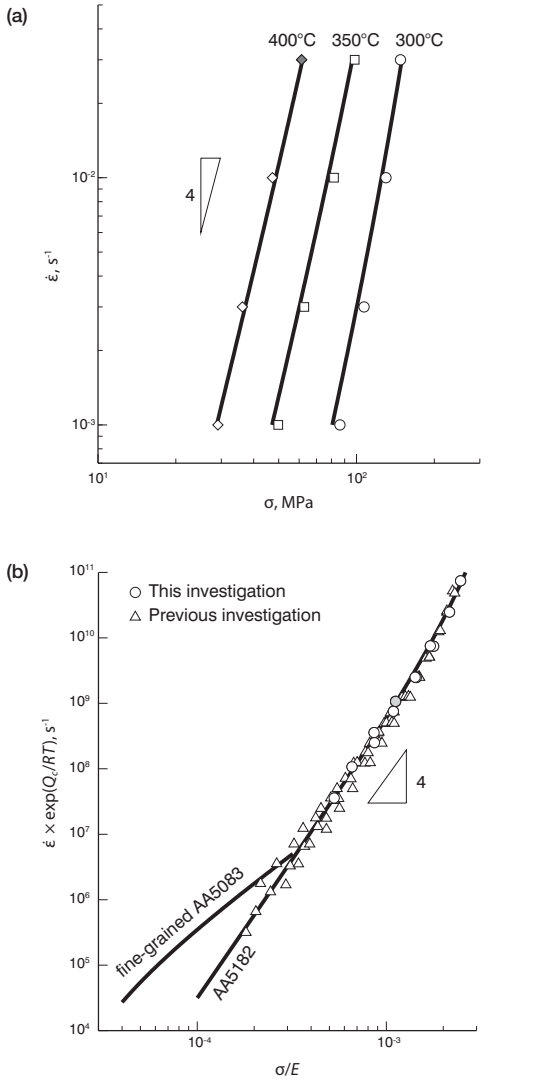

Fig.2 (a) True-strain rate is shown as a function of true flow stress on dual-logarithmic scales for a true strain of ε = 0.2 at three different temperatures. (b) Flow behavior from (a) is compared with data from prior studies of AA5182 [13)] and fine-grained AA5083 [7)] sheet materials in a plot of Zener-Hollomon parameter, assuming an activation energy of Q_c = 136 kJ/mole, against modulus-compensated flow stress. The filled symbol in each plot indicates the test condition used to investigate microstructure evolution.

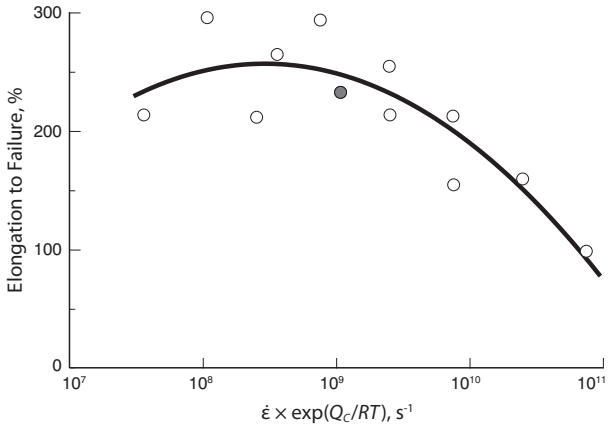

Fig.3 Elongation to fracture produced in the AA5182 material is plotted against Zener-Hollomon parameter assuming an activation energy of Q_c = 136 kJ/mole. The filled symbol indicates the value of Zener-Hollomon parameter used to investigate microstructure evolution.

Fig.2(b) presents the tensile data from Fig.2(a) as Zener-Hollomon parameter, $Z = \dot{\varepsilon} \exp(Q_c/RT)$, against modulus-compensated flow stress on dual-logarithmic scales, along with data for a different AA5182 material from a previous investigation [13] and a curve representing the trend of data from fine-grained AA5083 materials [7]. The values of Z are calculated for Fig.2(b) using an activation energy of Q_c = 136 kJ/mol. The data of Köster [38] for dynamic, unrelaxed, temperature-dependent elastic modulus of Al are used to compensate stress; the addition of Mg to Al has a negligible effect on elastic modulus [39]. The fine-grained, $d \approx 7$ μm, AA5083 materials exhibit superplastic deformation by GBS creep at low values of Z, but converge with the data of AA5182 materials as Z increases, when deformation is dominated by solute-drag creep. Behavior of the AA5182 material in the present investigation agrees very well with the results from a previous investigation of a similar material. The behavior of the AA5182 materials in Fig.2(b) is described well be an equation of the Garofalo type [27],

$$\dot{\varepsilon} = A \exp\left(\frac{-Q_c}{RT}\right)\left[\sinh\left(\alpha\frac{\sigma}{E}\right)\right]^n \qquad (2)$$

where $A = 7.37 \times 10^9$ s^{-1}, $\alpha = 526$, Q_c = 136 kJ/mol and n = 4.2. This modification of Equation 1 accounts for the effect of power-law breakdown, which occurs when $\dot{\varepsilon}/D > 10^{13}$ m^{-2} [27], or approximately $Z > 5 \times 10^8$ s^{-1} in this case. The curves shown for AA5182 in Fig.2 are from this fitted equation.

3.3 Tensile Ductility

Fig.3 presents tensile elongation as a function of Zener-Hollomon parameter for the AA5182 material. The large tensile elongations evident at low Z values, typically in excess of 200%, reflect the high formabilities possible in this material at elevated temperature, despite a grain size significantly larger than is typical of related superplastic materials [4]. These enhanced tensile ductilities are consistent with those reported for other non-superplastic Al-Mg low-impurity alloys and commercial materials [9), 11), 13)]. The drop in tensile ductility at high Z values, Z greater than approximately 10^9 s^{-1}, is a result of decreasing strain-rate sensitivity, as evident in Fig.2, which accelerates flow localization, i.e. necking. A decrease in tensile ductility is also expected at very low Z values, Z less than approximately 10^7 s^{-1}, because of an increasing propensity toward cavitation development [9), 11), 13), 40), 41)].

Fig.4 presents data for the Q-parameter as a function of Zener-Hollomon parameter. The Q-parameter, a convenient measure for the amount of flow localization which occurs at fracture in tension [40], compares the reduction-in-area (q) with the theoretical reduction-in-area in the absence of necking,

$$q^* = \left(1 - \frac{1}{1+e_f}\right) \qquad (3)$$

where e_f is the tensile elongation. The Q-parameter is then defined as $(q - q^*)/q^*$. A Q-parameter of greater than zero typically indicates flow localization, *i.e.* neck development, prior to fracture [40]. A Q-parameter of zero or less typically indicates fracture by cavity coalescence without significant flow localization [40]. As seen in Fig.4, the severity of flow localization increases with increasing Z value. This was used to advantage in the present investigation to study of the effect of strain on recrystallization and the production of abnormal grains.

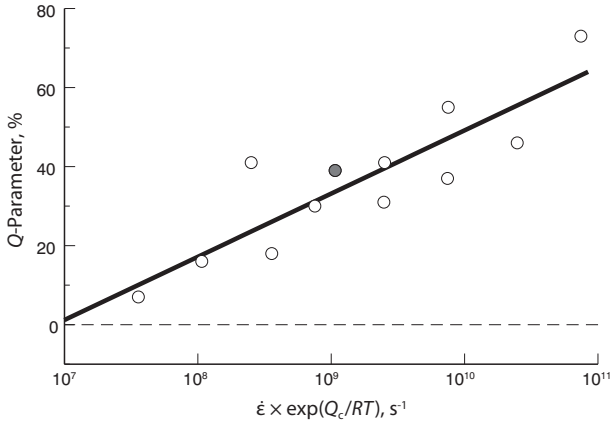

Fig.4 The Q-parameter is plotted against Zener-Hollomon parameter assuming an activation energy of Q_c = 136 kJ/mole. The filled symbol indicates the value of Zener-Hollomon parameter used to investigate microstructure evolution.

3.4 Microstructure Evolution

A series of tensile coupons were tested to a predetermined tensile elongation of 180% at a temperature of 400°C and a constant true-strain rate of 3×10^{-2} s^{-1} in order to create specimens with diffuse necks. These specimens were used to examine the effect of cooling and annealing treatments on microstructure. The diffuse neck in each specimen provides a range of strains, across which microstructure may be examined. The Z value corresponding to these test conditions, $Z = 1.08 \times 10^{9}$ s^{-1}, is shown by a filled symbol in Fig.2, Fig.3 and Fig.4. **Fig.5** shows examples of microstructures produced in specimens air cooled following tensile testing and approximate true strains at several locations in each specimen. The specimen shown in Fig.5(a) is as air-

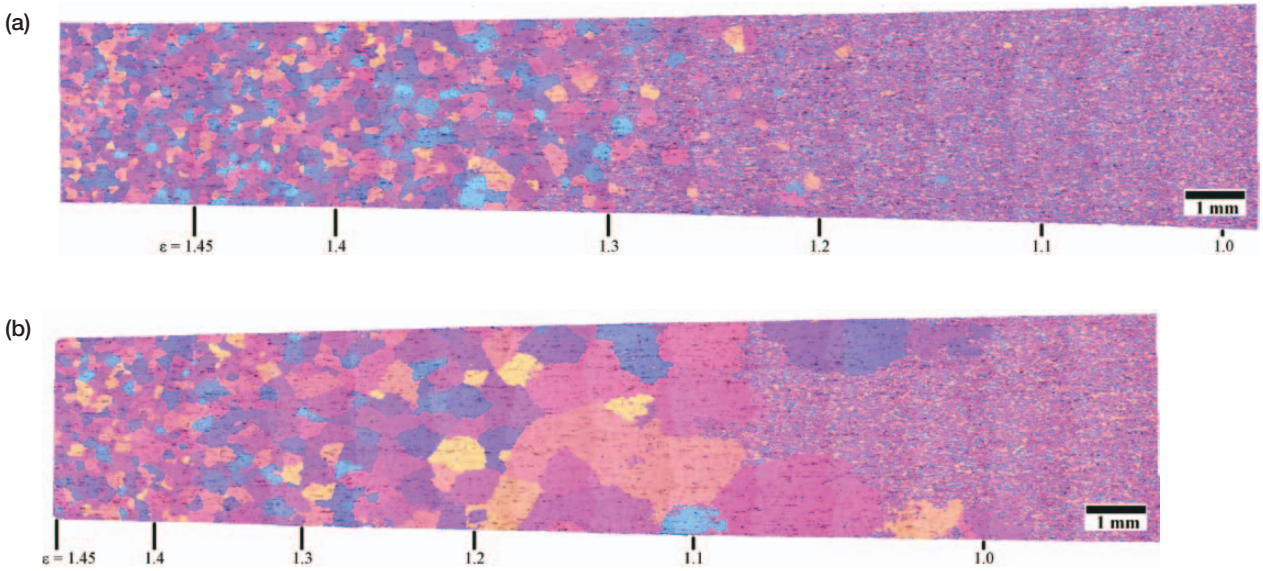

Fig.5 Optical photomicrographs from two halves of a single AA5182 tensile coupon are shown after tensile testing at 400°C and 3×10^{-2} s^{-1} to a tensile elongation of 180%. True strains, calculated from area reduction, are show at several locations. The specimen in the AC condition, shown in (a), was air cooled from the testing temperature. The specimen in the AC + A condition, shown in (b), was annealed at 400 for 1 hr. following air cooling from the testing temperature. (The tensile axis is horizontal.)
(a) AC
(b) AC + A

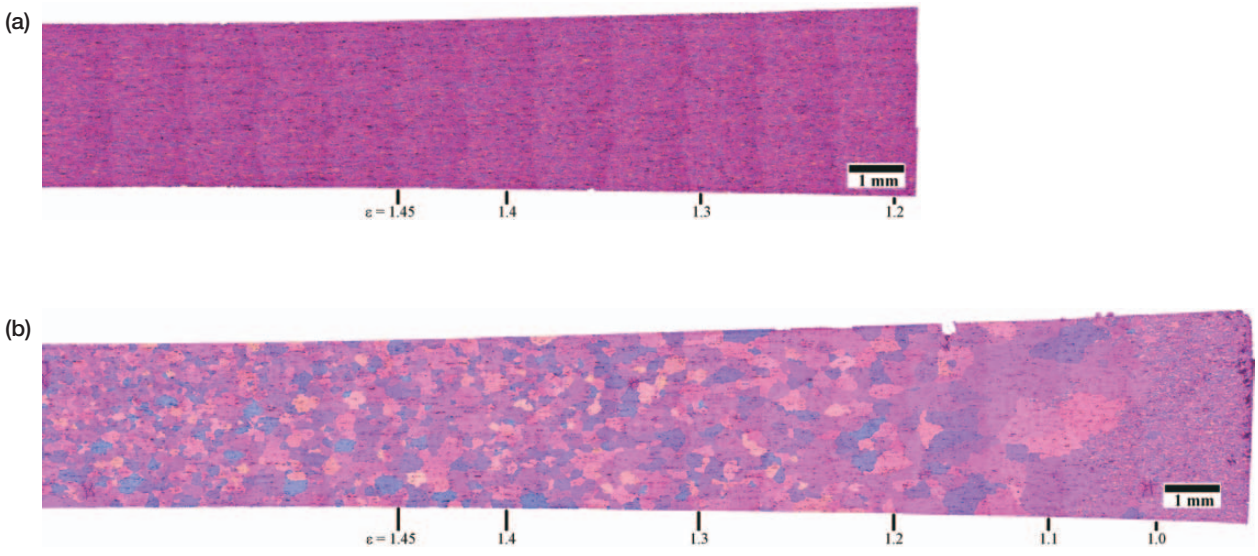

Fig.6 Optical photomicrographs are shown from a single AA5182 tensile coupon after tensile testing at 400°C and 3×10^{-2} s^{-1} to a tensile elongation of 180%. True strains, calculated from area reduction, are show at several locations. The specimen in the WQ condition, shown in (a), is as water quenched from the testing temperature immediately upon the completion of tensile straining. The specimen in the WQ + A condition, shown in (b), is the same specimen as shown in (a), but after annealing at 400°C for 1 hr. (The tensile axis is horizontal.)
(a) WQ
(b) WQ + A

cooled from the testing temperature. The left half of the specimen, where strain is the greatest, is fully recrystallized. However, isolated abnormal grains are evident within a matrix of unrecrystallized, deformed microstructure in the right half of the specimen, where the strain is less. These isolated abnormal grains duplicate the abnormal grains observed following hot forming of similar commercial Al-Mg materials [18), 19)], which motivated the present study. When a one-hour annealing treatment at the same temperature as the tensile test, 400°C, is subsequently applied, the microstructure exhibited in Fig.5(b) is produced. The microstructure in the left of the specimen, where strain is the greatest, is fully recrystallized and has a grain size similar to that produced at an identical strain directly after air cooling. The microstructure in the right of the specimen, where the strain is less, exhibits very large grains adjacent to an unrecrystallized microstructure. These large grains clearly result from growth into unrecrystallized microstructure by the isolated abnormal grains produced after air cooling, see Fig.5(a). This suggests that full recrystallization is a discontinuous process which occurs by abnormal grain growth.

The microstructures of Fig.5 give rise to a question of whether the formation of abnormal grains, and subsequent full recrystallization at the largest strains, occurred during deformation or during cooling after deformation was complete. To answer this question, specimens were water quenched immediately after the completion of deformation in the tensile test. **Fig.6**(a) presents a microstructure produced by water quenching immediately after tensile testing. Neither abnormal grains nor recrystallized microstructure are observed. Subsequent annealing of the quenched specimen shown in Fig.6(a) for one hour at the same temperature as the tensile test, 400°C, produced the microstructure shown in Fig.6(b). The subsequent annealing treatment produced a recrystallized microstructure in the regions of greatest strain and large, abnormal grains in the regions with lesser strains. Thus, it is proved that abnormal grain growth and recrystallization in AA5182 are suppressed during tensile deformation. In this case, abnormal grain growth and recrystallization are plainly static phenomena, in that they do not occur during plastic deformation, but during static annealing following deformation.

Images obtained by EBSD of a water-quenched specimen are presented in **Fig.7**. Fig.7(a) shows the microstructure of the undeformed specimen grip region after testing. This equiaxed microstructure is essentially the same as that of the as-received material prior to testing. Fig.7(b) shows the microstructure in the deformed specimen gage region as water-quenched after tensile testing. The local strain at the location of this image is $\varepsilon = 1.45$. This microstructure shows the expected elongation of grains along the tensile direction. Subgrains are clearly visible within these elongated grains. Subgrain diameters were measured from EBSD images and from OM images, and these measurements are reported

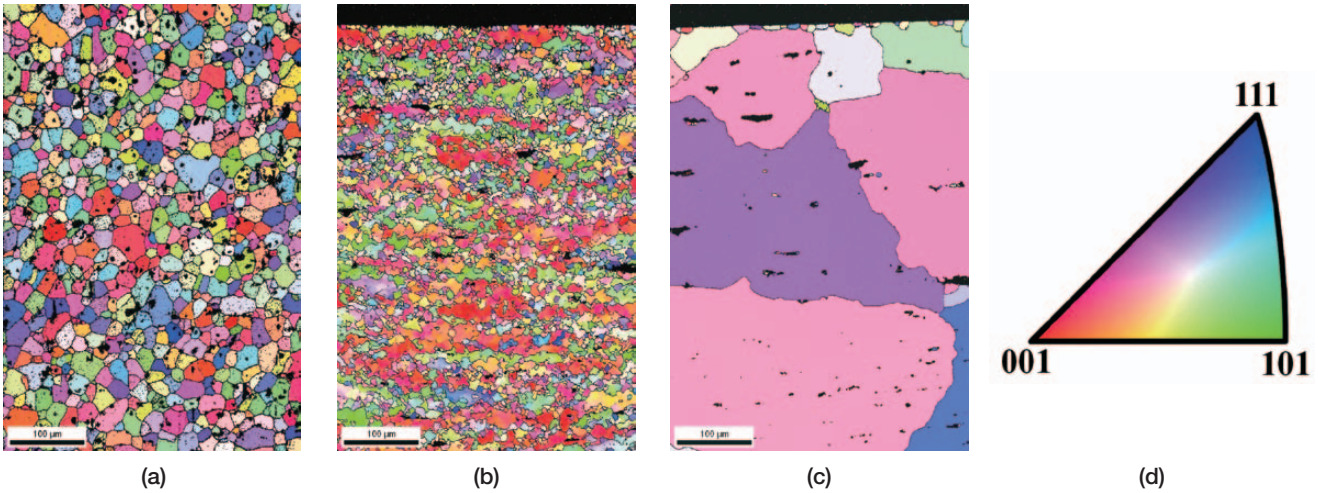

Fig.7 EBSD maps are shown for a specimen deformed at 400°C and 3×10^{-2} s^{-1} to an elongation of 180% and then water quenched upon the completion of tensile straining. Image (a) is from the undeformed grip region. Image (b) is from a position in the gage region deformed to an equivalent tensile true strain of 1.45 and immediately water quenched after testing. Image (c) is from the same specimen and the same area shown in image (b), but after subsequent annealing at 400°C for 1 hr., which produced abnormal grains. (The tensile axis is horizontal.)
(a) grip
(b) WQ at $\varepsilon = 1.45$
(c) WQ + A at $\varepsilon = 1.45$
(d) Color coded map

in **Table 4**. It is of note in Table 4 that the subgrain sizes measured from OM images are consistently larger than those from EBSD images. This is an expected difference between these measurement techniques, which has been addressed in the literature with respect to grain size measurements [31]. Because EBSD resolves more subgrain boundaries than does OM, subgrain sizes measured from EBSD images are consistently smaller than when measured from OM images. Having established this difference between measurement techniques, it can then be noted that the subgrain sizes shown in Table 4 are insensitive to strain, at least to within the standard deviations of the measurements. This is a result expected from Class I (Class A) alloys, which include AA5182, deformed under SD creep [34)~37), 42), 43)]. From these data, the subgrain size may be reasonably assumed to be constant across a wide range of strains for a given temperature and strain rate. Fig.7(c) shows an EBSD image of the same specimen as shown in (b), but after annealing at the tensile testing temperature, 400°C, for one hour. Complete recrystallization into much larger grains occurred during annealing.

Table 4 Lineal intercept subgrain diameters, λ, in specimens tested at a temperature of 400°C and a true-strain rate of 3×10^{-2} s^{-1} are shown as measured from optical microscope (OM) and EBSD images. The true strain, ε, from area reduction at the location of each measurement and the standard deviation, SD, of each measurement are provided.

Technique	ε	λ, μm	SD, μm
OM	0.5	7.4	±2
OM	1.3	6.9	±2
EBSD	1.18	5.3	±0.5
EBSD	1.45	5.4	±0.7

The texture developed during deformation was evaluated using EBSD measurements taken from the water-quenched specimen of Fig.7(b). Texture data are shown in **Fig.8** as (a) pole figures and (b) an orientation distribution function in Euler space using the Bunge notation. These data indicate that a two-component <100> + <111> fiber texture is developed in the AA5182 material during SD creep. These are the same principal texture components previously identified in AA5083 material following deformation by SD creep [31]. Beyond this consistency with the AA5083 data, the AA5182 data of Fig.8 also exhibit a weak cube texture.

4 DISCUSSION

The deformed microstructures (not recrystallized) shown in Fig.1(b), Fig.5, Fig.6 and Fig.7(b) exhibit the classical characteristics of geometric dynamic recrystallization (GDRX) [24), 25), 43)~46)]. These include elongation of grains (defined by high-angle boundaries) along the tensile axis, development of subgrains (defined by low-angle boundaries) throughout the elongated grains and polygonization of high-angle grain boundaries in conformance with the subgrain structure. GDRX is a continuous dynamic recrystallization process typically observed in Al-Mg alloys during hot deformation to large strains [24), 43), 44)]. For GDRX to run to completion, grain width must be reduced by straining until it is approximately equal to the subgrain size. At that point, subgrains are pinched off by the polygonized high-angle boundaries to form new grains of approximately the same size as the prior subgrains, but with high-angle boundaries. The schematic in **Fig.9** illustrates a deformed grain containing

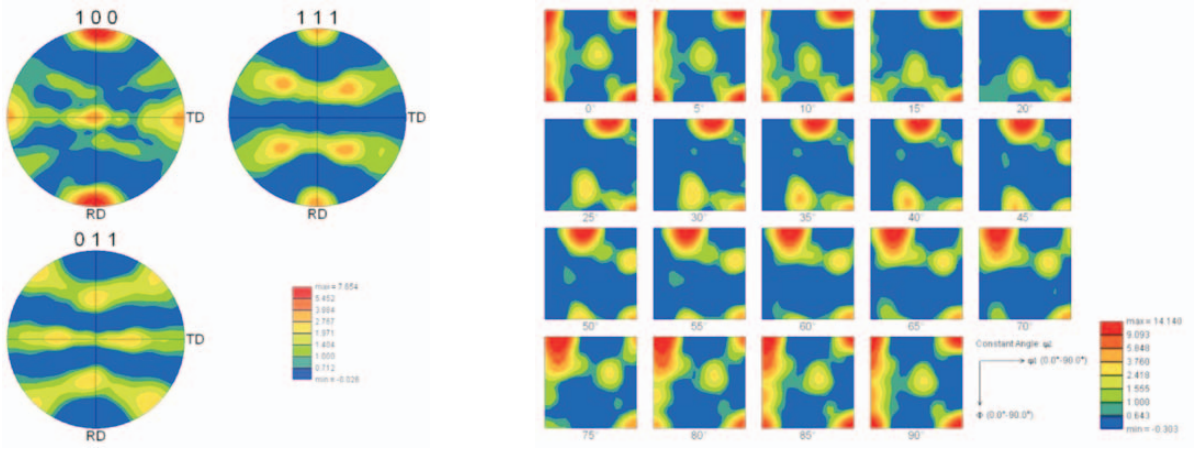

Fig.8 Texture data from EBSD measurements of the water-quenched specimen in Figure 7(b) are shown as (a) pole figures and (b) an orientation distribution function in Euler space using the Bunge notation.
(a) pole figures
(b) ODF

subgrains and having a polygonized grain boundary. This schematic is based on observed microstructure at a true strain of ε = 1.45 and demonstrates how microstructure developed during hot deformation proceeds through the GDRX process.

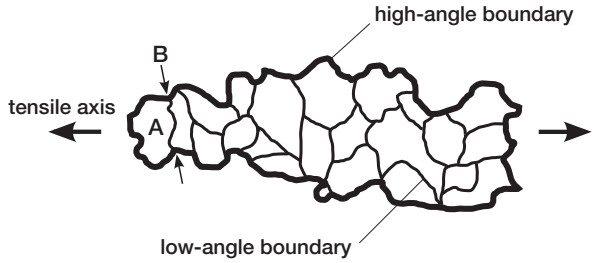

Fig.9 This schematic, based on observation of deformed microstructure at a true strain of ε = 1.45, illustrates the development of subgrains with low-angle boundaries within a deformed grain. With additional straining, the high-angle boundary will continue to polygonize in conformance with the subgrain structure until subgrains (such as A) pinch off (such as at B) to form new grains with high-angle boundaries, completing the GDRX process.

Based on a simple geometric analysis of grain deformation under uniaxial tension, the critical strain required for GDRX to run to completion may be calculated as [44],

$$\varepsilon_{GDRX} = 2\ln\left(\frac{d_0}{\lambda}\right) \quad (4)$$

where d_0 is the initial grain size and λ is the subgrain size. Measurements from OM observations, d_0 = 17μm and $\lambda \approx 7$ μm, suggest a critical strain for GDRX of ε_{GDRX} = 1.8. This strain is significantly larger than the strains at which abnormal grains are observed in the AA5182 material, as shown in Fig.5, Fig.6 and Fig.7. Abnormal grains are observed at true strains as small as 1.0 in the experiments, and complete recrystallization is observed at larger strains. Thus, GDRX alone cannot be responsible for the recrystallization phenomena nor the abnormal grains observed.

It is hypothesized that, although recrystallization is not by GDRX, the GDRX process does lead to nuclei for recrystallization. From a statistical point of view, individual subgrains will be pinched off by polygonized grain boundaries well before the critical strain for GDRX is reached. Such a case is illustrated in Fig.9, wherein the subgrain A is approaching a state in which it can be quickly pinched off at B to form a new grain. Indeed, the boundary of subgrain A already contains a much larger fraction of high-angle boundary, which can easily migrate, than it does low-angle boundary. Subgrain A may even grow by migration of the mobile high-angle portion of its boundary before pinch-off is complete. By this mechanism, the GDRX process may lead to nuclei, such as subgrain A, which can grow by static grain growth after deformation is complete. When the deformation strain is much less than the critical strain for GDRX, then only a few such nuclei will be created. For such a sparse population of nuclei, each nucleus will be surrounded by a large volume of deformed microstructure, which it may consume during growth. These nuclei may grow into abnormal grains during static annealing by the process of static abnormal grain growth (SAGG). During extended static annealing, SAGG may progress until the abnormal grains meet to form a completely recrystallized microstructure with a very large grain size. This is the case revealed in Fig.5(b) and Fig.6(b) at a strain of approximately 1.1. Thus, a discontinuous static recrystallization process involving grain growth can occur in a microstructure produced by GDRX, a continuous recrystallization process, when straining stops short of ε_{GDRX} and is followed by static annealing. As strain increases toward ε_{GDRX}, the number of nuclei created increases. This results in an increasingly fine recrystallized microstructure, until a minimum grain size is reached at a strain equal to the critical strain for GDRX. As the number of nuclei increases with strain, the grains produced by this recrystallization process may no longer be considered abnormal, *i.e.* unusually large. At this point, the SAGG terminology is no longer appropriate, and growth might be thought of in terms of a more usual recrystallization processes, or as simply static grain growth.

This hypothesis predicts several effects which may be tested against experimental data. First, abnormal grains will become evident at a strain just sufficient for the GDRX process to create a few nuclei capable of SAGG. This critical strain for SAGG, ε_{SAGG}, will be significantly less than the critical strain for GDRX to run to completion, ε_{GDRX}. As strain increases beyond the critical strain for SAGG, the number density of recrystallized grains will increase, and the recrystallized grain size will decrease. As strain approaches the critical strain for GDRX, the recrystallized grain size will reach a minimum grain size equivalent to that produced by GDRX. These predictions are tested against experimental data for recrystallized grain size and the number density of recrystallized grains taken at several strains within tested specimens. Measured values of recrystallized grain size are presented as a function of strain in **Fig.10**. **Fig.11** presents measurements of recrystallized grain number density as a function of strain.

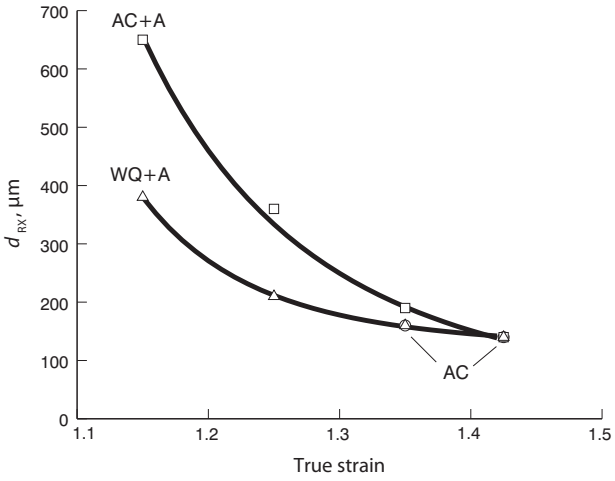

Fig.10 The lineal intercept grain size of recrystallized grains, d_{RX}, is shown as a function of strain for three different conditions of the AA5182 sheet following testing at 400°C and 3 ×10^{-2} s^{-1}.

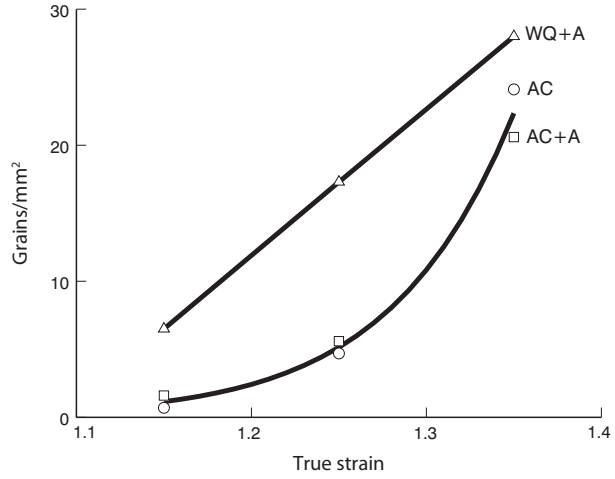

Fig.11 The area density of recrystallized grains is shown as a function of strain for three different conditions of the AA5182 sheet following testing at 400°C and 3 ×10^{-2} s^{-1}.

Fig.10 reveals that the size of recrystallized grains decreases with increasing strain, as predicted. Recrystallized grains vary in size from several hundreds of micrometers, which can easily be categorized as abnormal grains, to approximately 140 μm at the largest strain. No data for the annealed specimens (AC + A and WQ + A) are available at strains of less then 1.15 because too few recrystallized grains are available to make useful measurements. For the same reason, no data are available for the air-cooled specimen (AC) at strains of less than 1.35. The smallest grain size measured is significantly larger than the value predicted from GDRX theory of approximately the subgrain size, 7 μm. Although the greatest strains reached in the tested specimens, between 1.4 and 1.5, are significantly less than the strain calculated for completion of GDRX, ε_{GDRX} = 1.8, the minimum recrystallized grain size is still larger than what might be expected. Furthermore, the grain size appears to be approaching a minimum at the largest strains. This suggests that the microstructure produced by GDRX will not be stable at fine grain sizes, and the fine grain size predicted from GDRX theory may never be reached in practice for this material. This effect might limit the potential use of GDRX as a means for microstructure refinement.

At the largest strains, Fig.10 shows that all three specimens contain recrystallized grains of similar size. At lower strains, where data are not available for the AC condition, the AC + A specimen produces larger recrystallized grains than does the WQ + A specimen. This suggests that the AC + A specimen produced fewer nuclei for recrystallization than did the WQ + A specimen. In the proposed mechanism for nucleation of recrystallization followed by grain growth, the final grain size will be determined by the spacing between nuclei which can grow to consume the surrounding deformed microstructure. Fig.5(a) shows that recrystallization nuclei have formed and grown to become recrystallized grains during air cooling, while Fig.5(b) suggests that subsequent annealing simply allows the recrystallized grains, including abnormal grains, formed during air cooling to grow further. Fig.6(a) shows that no nuclei have grown, nor have even formed, during water quenching. Water quenching suppresses nucleation and forces it to occur during subsequent annealing at 400°C, which is sensible if nucleation occurs by recovery within individual subgrains that have been either pinched off or simply have a large fraction of high-angle boundary. In that case, nucleation requires sufficient temperature and time for recovery within individual subgrains, perhaps with a preferred texture component. Assuming this, nucleation during air cooling, such as in the AC and AC + A specimens of Fig.5, likely occurs at lower temperatures than does nucleation during the 400°C annealing treatment of the WQ + A specimen, resulting in fewer nuclei for recrystallization in the air-cooled specimens. The density of nuclei for recrystallization is equivalent to the density of abnormal grains or recrystallized grains, for which experimental data are presented in Fig.11. This figure clearly shows a significantly lower density of recrystallized grains in the specimens subjected to air cooling, compared to the WQ + A condition. Furthermore, the data of Fig.11 suggest that the critical strain for SAGG, the minimum strain for production of abnormal grains in the air-cooled specimen, is approximately ε_{SAGG} = 1.1. This result is important because it indicates that limiting forming strain to be less than this value will prevent

the occurrence of abnormal grains in components hot-formed in AA5182 sheet, at least for this temperature and strain rate.

One further prediction of the proposed mechanism was tested against experimental data. Equation 4 predicts that the critical strain for GDRX to run to completion will increase as the initial grain size increases. Thus, the strain necessary to initiate SAGG, *i.e.* create individual nuclei for recrystallization, will also increase as initial grain size increases. One tensile coupon of the AA5182 sheet material was statically annealed at 550°C for one hour, which produced grains of greater than one millimeter in size, see Table 2. This coupon was then tested in tension to fracture at a temperature of 400°C and a strain rate of 3×10^{-2} s^{-1}, followed by air cooling. Metallographic examination following testing revealed no recrystallized grains at strains of less than approximately 1.5, the maximum strain measured by area reduction at the fracture location. Recrystallized grains were evident only at the very greatest strains directly adjacent to the fracture surface of the failed specimen, as shown in **Fig.12**. Thus, abnormal grain formation can be suppressed during hot forming of the AA5182 sheet by obtaining a larger initial grain size. Of course, there are practical problems in using coarser grain sizes in commercial materials, such as developing inhomogeneities in strain, creating a rough "orange peel" surface and reducing service strength [9), 11), 13)].

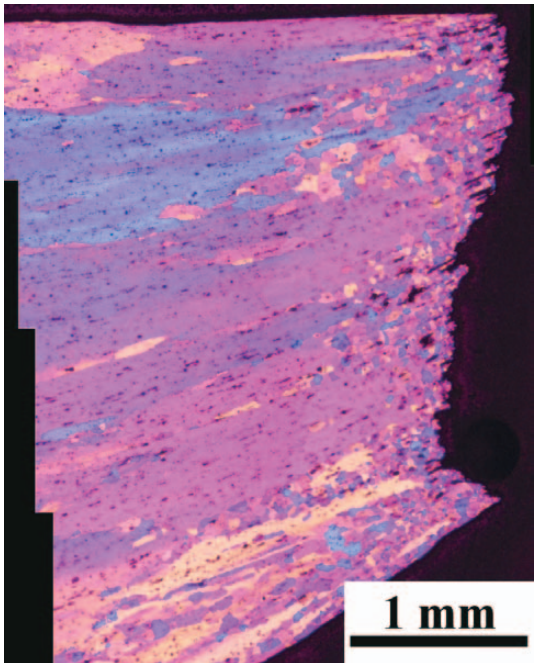

Fig.12 The location adjacent to the fracture surface, at the right, of a coarse-grained AA5182 specimen tested to fracture at 400°C and 3×10^{-2} s^{-1} is shown.

In this investigation, microstructure evolution data were produced from tests at only one temperature and one true-strain rate. Further study is warranted to investigate the effects of temperature, strain rate, annealing temperature and annealing time on abnormal grain production and recrystallization. Furthermore, the proposed mechanism of abnormal grain production and recrystallization would be expected to produce unique recrystallization textures. For example, grains of minority texture components can be preferred for abnormal grain growth [47)]. Additional investigations into recrystallization textures will be of interest. Data from such future studies will be useful to further test the validity of the proposed recrystallization mechanism.

An alternative to the terminology presented here is to define abnormal grain growth as distinct from recrystallization. That usage occurs in the literature. However, adhering to that definition requires a very awkward choice. One must either explain the evolution of abnormal grains, such as in Fig.1(b), by a mechanism that does not involve abnormal grain growth, or one must explain why the large grain in Fig.1(b) should not be considered an abnormal grain. The large grain in Fig.1(b) clearly fits the historical metallurgical definition of an abnormal grain, and it is most logical to consider that it has grown by abnormal grain growth. By considering abnormal grain growth to be part of a discontinuous recrystallization process, inconsistencies of terminology are avoided. Thus, it is recommended that abnormal grain growth not be considered necessarily distinct from recrystallization, but potentially a part of the discontinuous recrystallization process.

5 Conclusions

Abnormal grains observed following hot forming of Al-Mg commercial alloy AA5182 sheet have been reproduced in tensile coupons tested at 400°C and 3×10^{-2} s^{-1}. The formation of abnormal grains is suppressed during deformation and occurs only during static annealing following deformation. The growth of abnormal grains is, therefore, described as static abnormal grain growth, SAGG. This definition of SAGG, in conjunction with the recently-reported phenomenon of dynamic abnormal grain growth, DAGG [48)], defines a new categorization of abnormal grain growth phenomena which fits well with McQueen's taxonomy of recrystallization processes [25)]. The minimum strain required to produce abnormal grains, the critical strain for SAGG, is $\varepsilon_{SAGG} \approx 1.1$ under the conditions investigated. A mechanism is proposed to describe the production of grains susceptible to SAGG. This

mechanism requires elongation and polygonization of grains and development of subgrains with large fractions of high-angle boundary through the process of geometric dynamic recrystallization, GDRX. When deformation is terminated at a strain greater than ε_{SAGG}, but less than the strain necessary for the completion of GDRX, ε_{GDRX}, isolated subgrains with large fractions of high-angle boundary are created. These subgrains are the precursors of nuclei for recrystallization, and their density increases as strain increases from ε_{SAGG} up to ε_{GDRX}. After recovery during static annealing, some of these subgrains can grow by migration of the high-angle portions of their boundaries and, thus, become nuclei for recrystallization. At low strain accumulations, near ε_{SAGG}, these nuclei grow by SAGG to become the abnormal grains which motivated the present investigation. As nuclei density increases with increasing strain accumulation, the nucleated grains more easily grow to meet each other and produce a fully recrystallized microstructure; the grain size in that recrystallized microstructure decreases with increasing strain accumulation. In this manner, the normally continuous recrystallization process of GDRX is interrupted by the cessation of straining and is replaced with a discontinuous recrystallization process of limited recovery followed quickly by grain growth. This mechanism is consistent with experimental data for recrystallized grain size, recrystallized grain number density and the dependence of recrystallization on initial grain size. Aside from alloy modification [18), 20)], abnormal grains may be avoided after hot deformation of AA5182 sheet by: (1) limiting the forming strains to less than ε_{SAGG}, (2) rapid cooling immediately upon the completion of hot straining or (3) increasing the initial grain size of the sheet material. Among these, limiting the forming strain is the option of most practical value to commercial hot forming operations.

6 Acknowledgments

J.-K. Chang and E.M. Taleff gratefully acknowledge support for this work from the National Science Foundation (DMR-0605731), Nippon Steel Corp., Furukawa-Sky Aluminum Corp. and General Motors Corp.

This article was published in Metallurgical and Materials Transactions A Vol. **41A** (2010), 1942.

References

1) A. J. Barnes: Materials Science Forum, **170–172** (1994), 701.
2) A. J. Barnes: Materials Science Forum, **304–306** (1999), 785.
3) A. J. Barnes: Materials Science Forum, **357–359** (2001), 3.
4) T. G. Langdon: Materials Science and Engineering, **44** (2009), 5598.
5) O. D. Sherby and J. Wadsworth: Progress in Materials Science, **33** (1989), 169.
6) T. G. Langdon: Materials Science and Engineering, **A137** (1991), 1.
7) M.-A. Kulas, W. P. Green, E. M. Taleff, P. E. Krajewski and T. R. McNelley: Metallurgical and Materials Transactions A, **36A** (2005), 1249.
8) J. G. Schroth: in Advances in Superplasticity and Superplastic Forming, E. M. Taleff, P. A. Friedman, P. E. Krajewski, R. S. Mishra and J. G. Schroth, eds., TMS, Warrendale, PA (2004), 9.
9) E. M. Taleff, D. R. Lesuer and J. Wadsworth: Metallurgical and Materials Transactions A, **27A** (1996), 343.
10) M. Otsuka, S. Shibasaki and M. Kikuchi: Materials Science Forum, **233–234** (1997), 193.
11) E. M. Taleff, G. A. Henshall, T. G. Nieh, D. R. Lesuer and J. Wadsworth: Metallurgical and Materials Transactions A, **29A** (1998), 1081.
12) K. Takata, T. Ohwue, M. Saga and M. Kikuchi: Materials Science Forum, **331–337** (2000), 631.
13) E. M. Taleff, P. J. Nevland and P. E. Krajewski: Metallurgical and Materials Transactions A, **32A** (2001), 1119.
14) T. Ito, S. Shibasaki, M. Koma and M. Otsuka: Journal of the Institute of Metals, **66** (2002), 409.
15) T. Ito, M. Koma, S. Shibasaki and M. Otsuka: Journal of the Institute of Metals, **66** (2002), 476.
16) E. M. Taleff: in Advances in Superplasticity and Superplastic Forming. E. M. Taleff, P. A. Friedman, P. E. Krajewski, R. S. Mishra and J. G. Schroth, eds., TMS, Warrendale, PA, (2004), 85.
17) ASM Staff Writer. Advanced Materials & Processes, **163** (2005), 11.
18) H. Kazama, K. Nakao, K. Takata, O. Noguchi and Y. Suzuki: in Proceedings of the 108th Conference of the Japan Institute of Light Metals (Light Metals Conference 108th Spring Meeting), Japan Institute of Light Metals, Tokyo, Japan, 2005, 61.
19) F. Fukuchi, T. Yahaba, H. Akiyama, T. Ogawa, H. Iwasaki and I. Hori: Honda R&D Technical Review, **16** (2004), 23.
20) K. Shiotsuki, H. Akiyama, I. Hori, K. Kashiwazaki and S. Ueno: in Proceedings of the 107th Conference of the Japan Institute of Light Metals (Light Metals Conference 107th Spring Meeting), Japan Institute of Light Metals, Tokyo, Japan, (2004), 319.
21) F. J. Humphreys and M. Hatherly: Recrystallization and Related Annealing Phenomena. Elsevier, New York, (2004), 3.
22) J. G. Byrne: Recovery, Recrystallization and Grain Growth. The MacMillian Company, New York, (1965).
23) S. Agarwal, P. E. Krajewski and C. L. Briant. Metallurgical and Materials Transactions A, **39A** (2008), 1277.
24) D. Doherty, D. A. Hughes, F. J. Humphreys, J. J. Jonas, D. Juul Jensen, M. E. Kassner, W. E. King, T. R. McNelley, H. J. McQueen and A. D. Rollett: Materials Science and Engineering, **A238** (1997), 219.
25) H. J. McQueen: Development of Dynamic Recrystallization Theory. Materials Science and Engineering A, **387–389** (2004), 203.
26) "Standard Test Methods for Determining Average Grain Size." Standard Designation E 112–96, ASTM, 100 Barr Harbor Drive, West Conshohocken, PA 19428-2959, July (1996).
27) O. D. Sherby and P. M. Burke: Progress in Materials Science, **13** (1968), 325.
28) O. D. Sherby and E. M. Taleff: Materials Science and Engineering A, **A322** (2002), 89.

29) E. M. Taleff, W. P. Green, M.-A. Kulas, T. R. McNelley and P. E. Krajewski: Materials Science and Engineering A, **36** (2005), 1249.
30) E. M. Taleff: in Aluminum Wrought Products for Automotive, Packaging and Other Applications - The James Morris Honorary Symposium, S. K. Das, G. Jha, Z. Li, T. Zhai and J. Liu, eds., TMS, Warrendale, PA, (2006), 87.
31) T. R. McNelley, K. Oh-oishi, A. P. Zhilyaev, S. Swaminathan, P. E. Krajewski and E. M. Taleff: Metallurgical and Materials Engineering A, **39** (2008), 50.
32) P. Yavari, F. A. Mohamed and T. G. Langdon: Acta Metallurgica, **29** (1981), 1495.
33) P. Yavari and T. G. Langdon: Acta Metallurgica, **30** (1982), 2181.
34) J. Weertman: Journal of Applied Physics, **28** (1957), 1185.
35) J. Weertman: Trans. Metall. Soc. AIME, **218** (1960), .
36) W. R. Cannon and O. D. Sherby: Metallurgical Transactions A, **1** (1970), 1030.
37) F. A. Mohamed and T. G. Langdon: Acta Metallurgica, **22** (1974), 779.
38) W. Köster: Zeitschrift für Metallkunde, **39** (1948), 1.
39) K. Abe, Y. Tanji, H. Yoshinaga and S. Morozumi: Journal of Japan Institute of Light Metals, **27** (1977), 279.
40) M.-A. Kulas, W. P. Green, E. M. Taleff, P. E. Krajewski and T. R. McNelley: Metallurgical and Materials Transactions A, **37A** (2006), 645.
41) J.-K. Chang, E. M. Taleff and P. E. Krajewski: Metallurgical and Materials Transactions A, **A40** (2009), 3128.
42) M. E. Kassner, N. Q. Nguyen, G. A. Henshall and H. J. McQueen: Materials Science and Engineering, **A132** (1991), 97.
43) G. A. Henshall, M. E. Kassner and H. J. McQueen: Metallurgical Transactions A, **23A** (1992), 881.
44) F. J. Humphreys and M. Hatherly: Recrystallization and Related Annealing Phenomena. Elsevier, New York, (2004), 461.
45) H. J. McQueen, O. Knustad, N. Ryum and J. K. Solberg: Script Metallurgica, **19** (1985), 73.
46) A. Gholina, F. J. Humphreys and P. B. Prangnell: Acta Materialia, **50** (2002), 4461.
47) F. J. Humphreys and M. Hatherly: Recrystallization and Related Annealing Phenomena. Elsevier, New York, (2004), 375.
48) J. R. Ciulik and E. M. Taleff: Sripta Materialia, **61** (2009), 895.

Jung-Kuei Chang
Postdoctoral Fellow
Department of Mechanical Engineering
The University of Texas at Austin

Ken Takata
The Steel Research Laboratories
Nippon Steel Corp.

Koji Ichitani
Technical Research Division
Furukawa-Sky Aluminum Corp.

Eric M. Taleff
Professor
Department of Mechanical Engineering
The University of Texas at Austin